

Charge noise induced spin dephasing in a nanowire double quantum dot with spin-orbit coupling

Rui Li (李睿)^{1,*}

¹Key Laboratory for Microstructural Material Physics of Hebei Province,
School of Science, Yanshan University, Qinhuangdao 066004, China

(Dated: June 7, 2019)

Unexpected fluctuating charge field near a semiconductor quantum dot has severely limited the coherence time of the localized spin qubit. It is the interplay between the spin-orbit coupling and the asymmetrical confining potential in a quantum dot, that mediates a longitudinal interaction between the spin qubit and the fluctuating charge field. Here, we study the $1/f$ charge noise induced spin dephasing in a nanowire double quantum dot via exactly solving its eigenvalues and eigenfunctions. Our calculations demonstrate that the spin dephasing has a nonmonotonic dependence on the asymmetry of the double quantum dot confining potential. With the increase of the potential asymmetry, the spin dephasing first becomes stronger sharply then becomes weaker softly. Also, we find that the applied external magnetic field contributes to the spin dephasing, the dephasing is strongest at the anti-crossing point B_0 in the double quantum dot.

I. INTRODUCTION

The coherence of a quantum bit (qubit), an interesting phenomenon originates from the superposition of quantum states in quantum mechanics, has many applications in quantum computing and quantum information processing [1, 2]. Electron spin (or pseudo spin), localized in semiconductor quantum dot [3, 4], is an excellent qubit candidate due to its convenience for manipulation [5, 6] and scalability [7, 8] in experiments. Both the fast spin manipulation and the long spin coherence time are required to achieve a reliable quantum computer [2, 9]. Spin dephasing induced by unexpected environment noises is the primary obstacle limiting the potential applications of the spin qubit [10–13].

$1/f$ charge noise [14], an interesting environment noise whose spectrum density has a $1/f$ distribution, has been observed in various quantum nano-systems [15–18]. Recently, spin dephasing induced by $1/f$ charge noise was observed in a Si quantum dot integrated with micromagnet [19, 20]. The longitudinal slanting field created by the nearby micromagnet mediates a longitudinal spin-charge interaction that gives rise to the spin pure dephasing [21]. A detailed theoretical investigation on the underlying physics of the spin dephasing not only helps clarify the mysterious $1/f$ distribution mechanism, but also can guide how to improve the spin coherence time.

The spin-orbit coupling (SOC) [22], internally presented in III-V semiconductor materials, can mediate a transverse spin-charge interaction which leads to the well-known effect of the quantum dot electric-dipole spin resonance [23–26]. Recently, a longitudinal spin-charge interaction is demonstrated in a single quantum dot with both SOC and asymmetrical confining potential [27]. The longitudinal spin-charge interaction gives rise to the spin pure dephasing due to the $1/f$ charge noise [27]. Since

a double quantum dot (DQD) is usually used to produce a large transverse spin-charge interaction near its anti-crossing point, with applications in both spin manipulation [28] and cavity quantum electrodynamics [29, 30], it is of practical importance to study the $1/f$ charge noise induced spin dephasing in this system.

In this paper, the spin dephasing mechanism in a spin-orbit coupled nanowire DQD modeled by an infinite double square well is explored in detail. We find that a little asymmetry in the confining potential, e.g., several fractions of a milli-electron-volt in the potential difference or several nanometers in the width difference between the left and right dots of the DQD, can give rise to a remarkable spin dephasing. This would be instructive and meaningful to the quantum computing architecture based on semiconductor quantum dot, because it is almost impossible to produce exactly symmetrical quantum dot confining potential in experiments. A nonmonotonic dependence of the spin dephasing on the potential asymmetry is demonstrated. We also find the applied magnetic field contributes to the longitudinal spin-charge interaction, hence there is a sharp dip at the anti-crossing point B_0 in the dephasing versus magnetic field figure.

The paper is organized as follows. In Sec. II, we give the DQD model we are interested. In Sec. III, we calculate exactly the energy spectrum and the corresponding eigenfunctions of the DQD. In Sec. IV, the spin dephasing as a function of the potential asymmetry is studied in detail. In Sec. V, we demonstrate the spin dephasing also has a magnetic field dependence. At last, we give a brief summary in Sec. VI.

II. THE NANOWIRE DQD

The DQD system with one electron confined has been investigated for a long time [31–35]. In the early development of quantum computing, a quantum dot charge qubit was proposed using the two localized charge states

* ruili@ysu.edu.cn

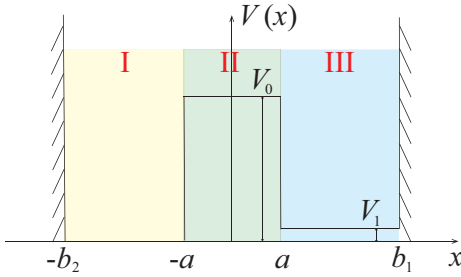


FIG. 1. The asymmetrical double-well potential used to mimic the confining potential of a nanowire DQD. The potential asymmetry can be tuned by varying either the potential difference V_1 between the dots or the width b_1 of the left dot.

in a DQD [36]. However, charge qubit is sensitive to external unexpected charge noise, such that its coherence time is usually very short [31, 37]. On the other hand, quantum dot spin qubit based on the spin degree of freedom of an electron, is less sensitive to external charge noise [38–40]. Also, in a DQD, it is easy to achieve a strong electric-dipole spin resonance, which is useful for the single qubit manipulation.

The one-dimensional square well problem in the presence of both the SOC and the Zeeman field is exactly solvable [27, 41–43]. In order to show explicitly the underlying physics of the spin dephasing and its dependence on the DQD parameters, here the confining potential of the nanowire DQD is modeled by an infinite double square well. The general double-well potential (see Fig. 1) with a little bit asymmetry reads

$$V(x) = \begin{cases} 0, & \text{region I: } -b_2 < x < -a, \\ V_0, & \text{region II: } -a < x < a, \\ V_1, & \text{region III: } a < x < b_1, \\ \infty, & \text{elsewhere.} \end{cases} \quad (1)$$

A conduction electron of the semiconductor material is localized in this double-well potential. The DQD Hamiltonian under investigation reads

$$H = \frac{p^2}{2m} + \alpha \sigma^z p + \Delta \sigma^x + V(x), \quad (2)$$

where m is the effective electron mass, α is the Rashba SOC strength [22], and $\Delta = g\mu_B B/2$ is half of the Zeeman splitting in the presence of an external magnetic field B . As emphasized in our previous study [27], the interplay between the SOC and the asymmetrical quantum dot confining potential can mediate a longitudinal spin-charge interaction, which gives rise to the spin pure dephasing. Here the potential asymmetry of the DQD can be tuned by varying either the parameter V_1 or parameter b_1 (see Fig. 1).

Our first step is to find the eigen-energies and the corresponding eigenfunctions of our model (2). The eigen-energies of a quantum system are determined by its boundary condition [44]. For the double-well potential we are considering, its boundary condition explicitly

TABLE I. The parameters of a InSb DQD used in our following calculations

m/m_0^a	α (eV Å) [45]	g	B_0 (T)
0.0136	1.05	50.6	0.05
a (nm)	b_1 (nm)	b_2 (nm)	V_0 (meV)
10	$55 \sim 60$	60	50
			V_1 (meV)
			$0 \sim 0.9$

^a m_0 is the free electron mass

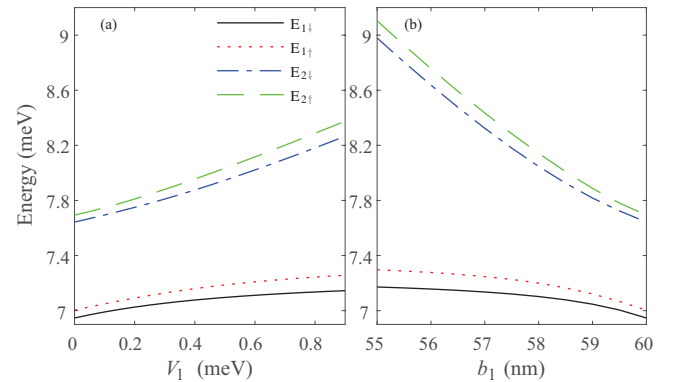


FIG. 2. The lowest four energy levels, labeled with the pseudo spin indices $|1 \downarrow\rangle$, $|1 \uparrow\rangle$, $|2 \downarrow\rangle$, and $|2 \uparrow\rangle$, in the DQD. (a) The energy levels as a function of the potential difference V_1 between the left and right dots. Here $b_1 = 60$ nm. (b) The energy levels as a function of the left dot width b_1 . Here $V_1 = 0$ meV.

reads [27]

$$\Psi(-b_2) = 0, \quad \Psi(\pm a - 0) = \Psi(\pm a + 0), \\ \Psi(b_1) = 0, \quad \Psi'(\pm a - 0) = \Psi'(\pm a + 0), \quad (3)$$

where $\Psi(x) = [\Psi_1(x), \Psi_2(x)]^T$ is the quantum dot eigenfunction to be determined and $\Psi'(x)$ is its first derivative. Here, $\Psi_{1,2}(x)$ are the two components of the eigenfunction due to the spin degree of freedom.

There is a strong Rashba SOC in the InSb material [45–47], such that here we only study in detail the spin dephasing in a InSb nanowire DQD, the physics in other III-V materials, such as InAs and GaAs, would be similar. In our following calculations, unless otherwise stated, the DQD parameters are given in Table I.

III. THE ENERGY SPECTRUM AND THE EIGENFUNCTIONS OF THE DQD

Following the standard method for tackling the square well problem with SOC [27, 42, 48, 49], we have obtained the energy spectrum and the corresponding eigenfunctions of our DQD model (2) exactly (the detailed method is given in Appendix A). By introducing 12 coefficients c_i ($i = 1, \dots, 12$) to be determined, we expand the eigenfunction in each coordinate region in terms of the corresponding bulk wavefunctions [see Eq. (A1)] [27, 42].

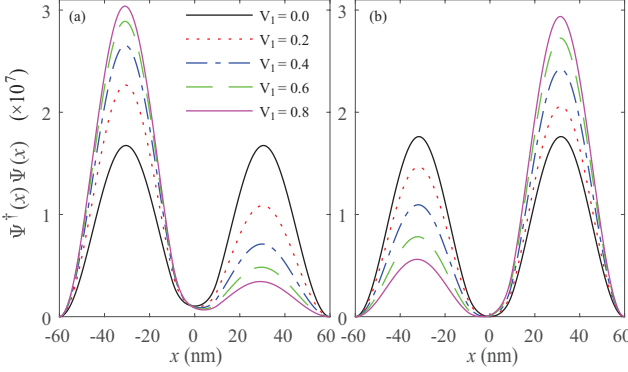


FIG. 3. The probability density distribution of the first eigenstate $|1\downarrow\rangle$ (a) and the third eigenstate $|2\downarrow\rangle$ (b) in the DQD with different potential difference V_1 between the left and right dots. Here $b_1 = 60.$

The boundary condition (3) actually contains 12 sub-equations. Therefore, substituting the eigenfunction in (3) with that given in (A1), we obtain a matrix equation $\mathbf{M} \cdot \mathbf{C} = 0$, where \mathbf{M} is a 12×12 matrix with E being its variable. The solutions of the transcendental equation $\det(\mathbf{M})=0$, an implicit equation of E , give the energy spectrum of the DQD. Once an eigen-energy, e.g., E_n , is obtained, we can solve its corresponding coefficients c_i^n by combining the equation $\mathbf{M} \cdot \mathbf{C} = 0$ with the normalization condition $\int dx \Psi_n^\dagger(x) \Psi_n(x) = 1$. Substituting the solved c_i^n into Eq. (A1), we then have the eigenfunction $\Psi_n(x)$ with eigenvalue E_n .

Note that because the spin is not a good quantum number in Hamiltonian (2), strictly speaking, the lowest Zeeman sublevels in the DQD encode a pseudo spin qubit (or spin-orbit qubit [46, 47]), not a spin qubit. Therefore, in this paper, the spin should be understood as a pseudo spin. Obviously, this pseudo spin contains a little orbital degree of freedom of the electron in a DQD in addition to the spin degree of freedom, such that the pseudo spin can respond to both the external magnetic and electric fields [50].

In a semiconductor DQD, the lowest four energy levels, labeled with $|1\downarrow\rangle$, $|1\uparrow\rangle$, $|2\downarrow\rangle$, and $|2\uparrow\rangle$, respectively, are relevant to the design of the pseudo spin qubit. The lowest four energy levels as a function of the potential asymmetry of the DQD are shown in Fig. 2. In Fig. 2(a), the potential asymmetry is tuned by varying the potential difference V_1 between the left and right dots. It should be noted that with the increase of V_1 , the level splitting of the pseudo spin $E_{1\uparrow} - E_{1\downarrow}$ becomes larger. In Fig. 2(b), the potential asymmetry is tuned by changing the width b_1 of the left dot. Similarly, with the decrease of b_1 , the level splitting of the pseudo spin $E_{1\uparrow} - E_{1\downarrow}$ also becomes larger.

Once the energy spectrum of the DQD is obtained, we can calculate the corresponding eigenfunctions. The probability density distribution of states $|1\downarrow\rangle$ and $|2\downarrow\rangle$ with various potential differences V_1 and various left dot

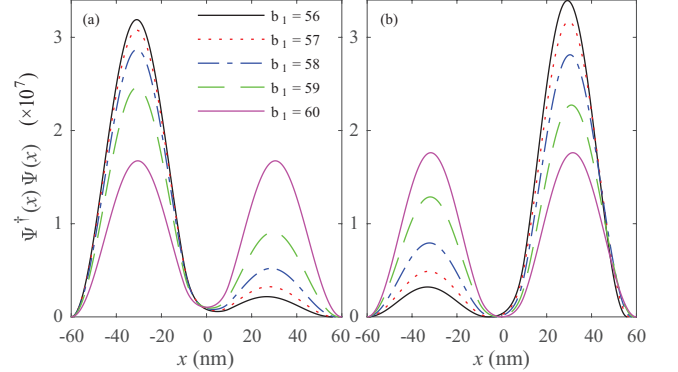


FIG. 4. The probability density distribution of the first eigenstate $|1\downarrow\rangle$ (a) and the third eigenstate $|2\downarrow\rangle$ (b) in the DQD with different left dot width b_1 . Here $V_1 = 0$ meV.

widths b_1 are shown in Figs. 3 and 4, respectively. The probability density distribution of state $|1\uparrow\rangle$ is similar to that of $|1\downarrow\rangle$, and the probability density distribution of state $|2\uparrow\rangle$ is similar to that of $|2\downarrow\rangle$, are not shown here. If the confining potential is symmetrical, i.e., $V_1 = 0$ meV in Fig. 3 or $b_1 = 60$ nm in Fig. 4, the probability density distribution is symmetrical with respect to the $x = 0$ axis. Once the potential asymmetry is presented, the symmetrical probability density distribution is broken. Also, with the increase of the potential asymmetry of the DQD, i.e., via increasing V_1 or shortening b_1 , the ground state $|1\downarrow\rangle$ in the DQD becomes more localized to one of the dot [see Figs. 3(a) and 4(a)], i.e., the probability density in the left dot is larger than that in the right dot. This is also the reason why the energy splitting $E_{1\uparrow} - E_{1\downarrow}$ becomes larger when the potential asymmetry is tuned to large in Fig. 2. When the orbital wavefunction is more un-localized, the spin-orbit effects in the system are much stronger [25, 42, 51].

IV. THE SPIN PURE DEPHASING

The transverse interaction between a quantum dot spin qubit and an external driving electric field has been demonstrated a decade ago. The representative example is the quantum dot electric-dipole spin resonance [23–26, 52, 53]. However, the transverse spin-charge interaction can only lead to possible spin relaxation [54]. Recently, a longitudinal spin-charge interaction, which induces the spin pure dephasing due to the external charge noise, has been demonstrated in a single quantum dot with both SOC and asymmetrical confining potential [27].

$1/f$ charge noise, the spectrum density of which is inversely proportional to the noise frequency, has attracted considerable interests for many decades [12–14, 55, 56]. Here we study the $1/f$ charge noise induced spin pure dephasing in a nanowire DQD. Following the method in deriving the interaction Hamiltonian of a two-level

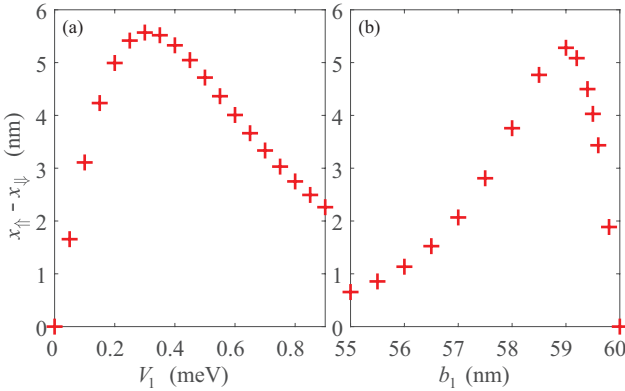


FIG. 5. (a) The difference $x_{\uparrow} - x_{\downarrow}$ for the case shown in Fig. 2(a) as a function of the potential difference V_1 between the left and right dots. (b) The difference $x_{\uparrow} - x_{\downarrow}$ for the case shown in Fig. 2(b) as a function of the right dot width b_1 .

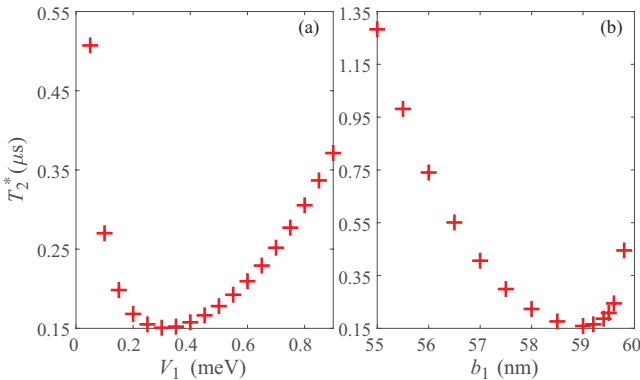


FIG. 6. The coherence time T_2^* as a function of the potential asymmetries. (a) The T_2^* as a function of the potential difference V_1 between the left and right dots. (b) The T_2^* as a function of the right dot width b_1 .

system with a bosonic noise [57], here we construct a model of the spin qubit interacting with the $1/f$ charge noise. The fluctuating charge field can be expressed as $\mathbf{E} = \sum_k \Xi_k \hat{e}_k (b_k + b_k^\dagger)$, where Ξ_k is the charge field in the wavevector space, \hat{e}_k is an unit vector. Hence, the total Hamiltonian describing spin-noise interaction reads

$$H_{\text{tot}} = H + ex \cos \Theta \sum_k \Xi_k (b_k + b_k^\dagger) + \sum_k \hbar \omega_k b_k^\dagger b_k, \quad (4)$$

where $\cos \Theta = \hat{x} \cdot \hat{e}_k$, for simplicity, we have assumed $\hat{e}_k = \hat{e}$ does not depend on k . When we focus only on the Hilbert subspace spanned by the qubit basis states: $|1\uparrow\rangle$ and $|1\downarrow\rangle$, the longitudinal qubit-noise interaction is characterized by the difference between $x_{\uparrow} = \langle 1\uparrow | x | 1\uparrow \rangle$ and $x_{\downarrow} = \langle 1\downarrow | x | 1\downarrow \rangle$ [27]. In this case, the total

Hamiltonian can be reduced to

$$H_{\text{tot}} = \frac{E_{1\uparrow} - E_{1\downarrow}}{2} \tau^z + \sum_k \hbar \omega_k b_k^\dagger b_k + \sum_k e \Xi_k \left(\frac{x_{\uparrow} - x_{\downarrow}}{2} \tau^z + \frac{x_{\uparrow} + x_{\downarrow}}{2} \right) (b_k + b_k^\dagger) \cos \Theta, \quad (5)$$

where $\tau^z = |1\uparrow\rangle\langle 1\uparrow| - |1\downarrow\rangle\langle 1\downarrow|$ is the Pauli z matrix. As can be seen clearly from the above equation, if $x_{\uparrow} = x_{\downarrow}$, the qubit cannot longitudinally couple to the charge noise. Therefore, the emergence of the phase noise is due to the following general reason, the average value of electric-dipole operator ex in one Zeeman sublevel $|1\downarrow\rangle$ is different from that in the other Zeeman sublevel $|1\uparrow\rangle$.

In Fig. 5, we show the difference $x_{\uparrow} - x_{\downarrow}$ as a function of the potential asymmetries of the DQD. Interestingly, we find the difference $x_{\uparrow} - x_{\downarrow}$ has a nonmonotonic dependence on the potential asymmetries. Note that we can tune the potential asymmetry to large by either increasing V_1 or shortening b_1 (see Fig. 1). There is a critical potential difference V_1^c (see Fig. 5(a)) or a critical left dot width b_1^c (see Fig. 5(b)), at which the difference $x_{\uparrow} - x_{\downarrow}$ becomes maximal. Also, the calculated difference $x_{\uparrow} - x_{\downarrow}$ is in the nanometer scale for the DQD parameters we choose. It is easy to produce a larger $x_{\uparrow} - x_{\downarrow}$ in the DQD, in comparison with results in a single quantum dot [27]. Also, at $V_1 = 0$ meV in Fig. 5(a) or $b_1 = 60$ nm in Fig. 5(b), the difference $x_{\uparrow} - x_{\downarrow}$ is exactly zero, this is because in these cases the model (2) has a Z_2 symmetry as discussed in Ref. [27].

The phase coherence of the spin qubit is described by the off-diagonal element of the qubit density matrix. If we model the phase coherence as $|\rho_{\uparrow\downarrow}(t)/\rho_{\uparrow\downarrow}(0)| = \exp(-\Gamma(t))$, the decay factor has the following exact expression [58]

$$\Gamma(t) \equiv \langle \Gamma(t) \rangle_{\Theta} = \frac{(x_{\uparrow} - x_{\downarrow})^2}{2(b_2 - a)^2} \int_{\omega_{\text{min}}}^{\omega_{\text{max}}} S(\omega) \frac{\sin^2(\omega t/2)}{(\omega/2)^2}, \quad (6)$$

where

$$S(\omega) = \sum_k \frac{e^2 \Xi_k^2 (b_2 - a)^2 k_B T}{\hbar^2 \omega} \delta(\omega - \omega_k) \equiv \frac{A^2}{\omega}$$

is the noise spectrum function, with A being the spectrum strength. Here, we have also introduced both a low frequency ω_{min} and a high frequency ω_{max} cut-offs [59]. In addition, the bosonic occupation number in thermal equilibrium is reduced as $n(\omega) = 1/(\exp(\hbar\omega/k_B T) - 1) \approx k_B T/\hbar\omega$ for all the low frequency charge noise mode [21]. Following our previous study, we choose $A = 20$ MHz [27], $\omega_{\text{min}} = 0.01$ Hz [20] and $\omega_{\text{max}} = 5 \times 10^5$ Hz [20] in our following calculations.

The phase coherence time T_2^* of the spin qubit is given by solving the equation $\Gamma(T_2^*) = 1$, i.e., at time T_2^* , the coherence is reduced from 1 to e^{-1} . In Fig. 6, we show the coherence time T_2^* as a function of the asymmetrical potential parameters of the DQD. As expected, as a

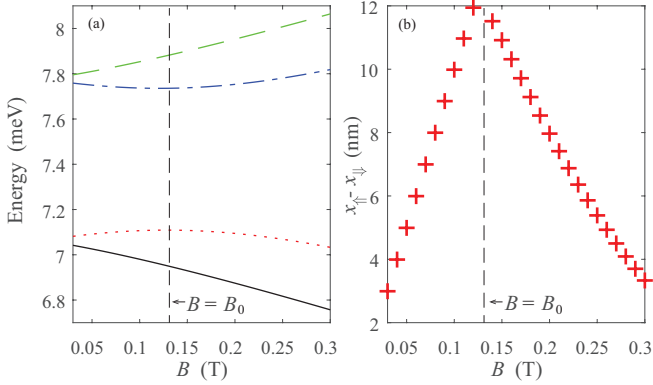


FIG. 7. (a) The lowest four energy levels in the DQD as a function of the applied magnetic field near the anti-crossing point. (b) The difference $x_↑ - x_↓$ as a function of the applied magnetic field. Here $V_1 = 0.2$ meV and $b_1 = 60$ nm.

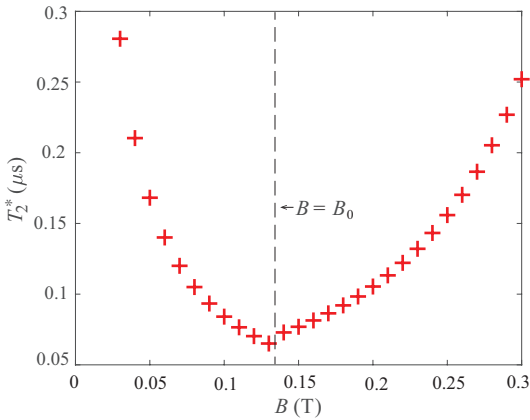


FIG. 8. The phase coherence time T_2^* as a function of the applied magnetic field B . Here $V_1 = 0.2$ meV and $b_1 = 60$ nm.

consequence of the results given in Fig. 5, the phase coherence time T_2^* also has a nonmonotonic dependence on the asymmetrical parameters V_1 or b_1 of the DQD. The coherence time T_2^* has minimal value at the critical potential parameter V_1^c (see Fig. 6(a)) or b_1^c (see Fig. 6(b)). Also, when the confining potential is symmetrical, i.e., $V_1 = 0$ meV in Fig. 6(a) or $b_1 = 60$ nm in Fig. 6(b), there is no spin dephasing $T_2^* = \infty$ as already illustrated in Fig. 5. As can be seen, a little asymmetry in the DQD confining potential can result in a large spin dephasing.

V. THE MAGNETIC FIELD DEPENDENCE OF DEPHASING

It is well-known there is an anti-crossing structure [32] in the energy versus magnetic field plot of the DQD. Near the anti-crossing point B_0 , the spin and orbital degrees of freedom of the electron are highly hybridized, such that a strong electric-dipole spin resonance [60] or a strong

spin-cavity interaction [29, 30] can be achieved near this point. One interesting question is how the magnetic field affects the spin dephasing in the DQD.

In many cases of the spin pure dephasing, the magnetic field only affects the Zeeman splitting of the electron [38, 39], thus does not contribute to the spin dephasing. However, in the spin dephasing mechanism mediated by the interplay between the SOC and the asymmetrical confining potential, the magnetic field obviously plays a more complicated role. The magnetic field here not only gives rise to a Zeeman splitting in the DQD, but also contributes to the spin-charge interaction, especially near the anticrossing point.

We show the lowest four energy levels in the DQD as a function of the applied magnetic field B in Fig. 7(a). The level anticrossing can be clearly seen. The energy gap is about 0.63 meV, very large due to the strong SOC in the InSb material. The magnitude of this gap reflects the strength of the SOC in the material. We also calculate the difference of the average values of the dipole operator x between the lowest Zeeman sublevels $|1 \uparrow\rangle$ and $|1 \downarrow\rangle$ near the anti-crossing point (see Fig. 7(b)). As expected, there is a sharp peak at the anti-crossing point in the $x_↑ - x_↓$ versus B plot. It is reasonable when we tune the magnetic field away from the anticrossing point, $x_↑ - x_↓$ becomes smaller.

It follows that the phase coherence time T_2^* also has a similar dependence on the magnetic field B (see Fig. 8), except that the peak structure is changed to a dip structure. Before the anti-crossing point, with the increase of the field, T_2^* becomes smaller, while after the anticrossing point, with the increase of the field, T_2^* becomes larger instead. The minimum of T_2^* is located at the anticrossing magnetic field B_0 , where there is a strongest spin dephasing.

VI. SUMMARY

In summary, the theory of the $1/f$ charge noise induced spin dephasing in a nanowire DQD is built explicitly in this paper. The interplay between the SOC and the asymmetrical confining potential mediates a longitudinal spin-charge interaction in the DQD. The spin dephasing is not monotonically dependent on the degree of the asymmetry of the potential. The applied external magnetic field not only gives rise to the electron Zeeman splitting, but also contribute to the spin-charge interaction, hence the spin is severely dephased near the anti-crossing point B_0 in the DQD.

ACKNOWLEDGEMENTS

This work is supported by the National Natural Science Foundation of China Grant No. 11404020, the Postdoctoral Science Foundation of China Grant No. 2014M560039, the Project from the Department of

Education of Hebei Province Grant No. QN2019057,

and the Starting up Foundation from Yanshan University Grant No. BL18043.

Appendix A: The derivation of the transcendental equation

We first solve the continuous spectrum of the bulk Hamiltonian $H_0 = \frac{p^2}{2m} + \alpha\sigma^z p + \Delta\sigma^x$ in the absence of the hard wall boundary condition. The explicit dispersion relation and the bulk wavefunctions can be found elsewhere [27, 42]. Now, we can write the eigenfunction in the quantum dot as follows

$$\Psi(x) = \begin{cases} c_1 \begin{pmatrix} \cos \frac{\theta_1}{2} \\ \sin \frac{\theta_1}{2} \end{pmatrix} e^{ik_1 x} + c_2 \begin{pmatrix} \sin \frac{\theta_1}{2} \\ \cos \frac{\theta_1}{2} \end{pmatrix} e^{-ik_1 x} + c_3 \begin{pmatrix} \sin \frac{\theta_2}{2} \\ -\cos \frac{\theta_2}{2} \end{pmatrix} e^{ik_2 x} + c_4 \begin{pmatrix} \cos \frac{\theta_2}{2} \\ -\sin \frac{\theta_2}{2} \end{pmatrix} e^{-ik_2 x}, & \text{I} \\ c_5 \begin{pmatrix} 1 \\ Re^{i\Phi} \end{pmatrix} e^{ik_x x - k_y x} + c_6 \begin{pmatrix} Re^{-i\Phi} \\ 1 \end{pmatrix} e^{-ik_x x - k_y x} + c_7 \begin{pmatrix} 1 \\ Re^{-i\Phi} \end{pmatrix} e^{ik_x x + k_y x} + c_8 \begin{pmatrix} Re^{i\Phi} \\ 1 \end{pmatrix} e^{-ik_x x + k_y x}, & \text{II} \\ c_9 \begin{pmatrix} \cos \frac{\theta_3}{2} \\ \sin \frac{\theta_3}{2} \end{pmatrix} e^{ik_3 x} + c_{10} \begin{pmatrix} \sin \frac{\theta_3}{2} \\ \cos \frac{\theta_3}{2} \end{pmatrix} e^{-ik_3 x} + c_{11} \begin{pmatrix} \sin \frac{\theta_4}{2} \\ -\cos \frac{\theta_4}{2} \end{pmatrix} e^{ik_4 x} + c_{12} \begin{pmatrix} \cos \frac{\theta_4}{2} \\ -\sin \frac{\theta_4}{2} \end{pmatrix} e^{-ik_4 x}, & \text{III} \end{cases} \quad (\text{A1})$$

where

$$\begin{aligned} k_{1,2} &= \sqrt{2}m\alpha \sqrt{1 + \frac{E}{m\alpha^2} \mp \sqrt{1 + 2\frac{E}{m\alpha^2} + \frac{\Delta^2}{m^2\alpha^2}}}, \quad \theta_{1,2} = \arctan(\Delta/(\alpha k_{1,2})), \\ k_{x,y} &= m\alpha \sqrt{\pm 1 \pm \frac{E - V_0}{m\alpha^2} + \sqrt{\frac{(E - V_0)^2 - \Delta^2}{m^2\alpha^4}}}, \quad R \cos \Phi = -\frac{m\alpha^2 + \alpha k_x}{\Delta}, \quad R \sin \Phi = -\frac{k_x k_y + m\alpha k_y}{m\Delta}, \\ k_{3,4} &= \sqrt{2}m\alpha \sqrt{1 + \frac{E - V_1}{m\alpha^2} \mp \sqrt{1 + 2\frac{E - V_1}{m\alpha^2} + \frac{\Delta^2}{m^2\alpha^2}}}, \quad \theta_{3,4} = \arctan(\Delta/(\alpha k_{3,4})). \end{aligned} \quad (\text{A2})$$

We totally have 12 coefficients c_i ($i = 1, \dots, 12$) to be determined. The boundary condition (3) actually has 12 subequations. Therefore, when $\Psi(x)$ in Eq. (3) is replaced with the above expanded form, we obtain the following matrix equation

$$\mathbf{M} \cdot \mathbf{C} = 0. \quad (\text{A3})$$

where \mathbf{M} is 12×12 matrix and $\mathbf{C} = [c_1, c_2, \dots, c_{12}]^T$. If the above equation array has non-trivial solutions, the determinant of matrix \mathbf{M} must be zero, i.e.,

$$\det(\mathbf{M}) = 0. \quad (\text{A4})$$

This transcendental equation is actually an implicit equation of the eigen-energy E . Solving this equation, we obtain the energy spectrum of the DQD. Once an eigen-value E_n is obtained, we can solve the coefficients c_i^n ($i=1, \dots, 12$) via Eq. (A3). Hence, the corresponding eigenfunctions $\Psi_n(x)$ with eigen value E_n can be determined from Eq. (A1).

The detailed matrix elements of \mathbf{M} read

$$\begin{aligned}
M_{1,1} &= e^{-ik_1 b_2} \cos \frac{\theta_1}{2}, \quad M_{1,2} = e^{ik_1 b_2} \sin \frac{\theta_1}{2}, \quad M_{1,3} = e^{-ik_2 b_2} \sin \frac{\theta_2}{2}, \quad M_{1,4} = e^{ik_2 b_2} \cos \frac{\theta_2}{2}, \\
M_{1,5} &= M_{1,6} = M_{1,7} = M_{1,8} = M_{1,9} = M_{1,10} = M_{1,11} = M_{1,12} = 0, \\
M_{2,1} &= e^{-ik_1 b_2} \sin \frac{\theta_1}{2}, \quad M_{2,2} = e^{ik_1 b_2} \cos \frac{\theta_1}{2}, \quad M_{2,3} = -e^{-ik_2 b_2} \cos \frac{\theta_2}{2}, \quad M_{2,4} = -e^{ik_2 b_2} \sin \frac{\theta_2}{2}, \\
M_{2,5} &= M_{2,6} = M_{2,7} = M_{2,8} = M_{2,9} = M_{2,10} = M_{2,11} = M_{2,12} = 0, \\
M_{3,1} &= e^{-ik_1 a} \cos \frac{\theta_1}{2}, \quad M_{3,2} = e^{ik_1 a} \sin \frac{\theta_1}{2}, \quad M_{3,3} = e^{-ik_2 a} \sin \frac{\theta_2}{2}, \quad M_{3,4} = e^{ik_2 a} \cos \frac{\theta_2}{2}, \quad M_{3,5} = -e^{-ik_x a + k_y a}, \\
M_{3,6} &= -Re^{-i\Phi + ik_x a + k_y a}, \quad M_{3,7} = -e^{-ik_x a - k_y a}, \quad M_{3,8} = -Re^{i\Phi + ik_x a - k_y a}, \quad M_{3,9} = M_{3,10} = M_{3,11} = M_{3,12} = 0, \\
M_{4,1} &= e^{-ik_1 a} \sin \frac{\theta_1}{2}, \quad M_{4,2} = e^{ik_1 a} \cos \frac{\theta_1}{2}, \quad M_{4,3} = -e^{-ik_2 a} \cos \frac{\theta_2}{2}, \quad M_{4,4} = -e^{ik_2 a} \sin \frac{\theta_2}{2}, \\
M_{4,5} &= -Re^{i\Phi - ik_x a + k_y a}, \quad M_{4,6} = -e^{ik_x a + k_y a}, \quad M_{4,7} = -Re^{-i\Phi - ik_x a - k_y a}, \quad M_{4,8} = -e^{ik_x a - k_y a}, \\
M_{4,9} &= M_{4,10} = M_{4,11} = M_{4,12} = 0, \\
M_{5,1} &= M_{5,2} = M_{5,3} = M_{5,4} = 0, \quad M_{5,5} = e^{ik_x a - k_y a}, \quad M_{5,6} = Re^{-i\Phi - ik_x a - k_y a}, \quad M_{5,7} = e^{ik_x a + k_y a}, \\
M_{5,8} &= Re^{i\Phi - ik_x a + k_y a}, \quad M_{5,9} = -e^{ik_3 a} \cos \frac{\theta_3}{2}, \quad M_{5,10} = -e^{-ik_3 a} \sin \frac{\theta_3}{2}, \\
M_{5,11} &= -e^{ik_4 a} \sin \frac{\theta_4}{2}, \quad M_{5,12} = -e^{-ik_4 a} \cos \frac{\theta_4}{2}, \\
M_{6,1} &= M_{6,2} = M_{6,3} = M_{6,4} = 0, \quad M_{6,5} = Re^{i\Phi + ik_x a - k_y a}, \quad M_{6,6} = e^{-ik_x a - k_y a}, \quad M_{6,7} = Re^{-i\Phi + ik_x a + k_y a}, \\
M_{6,8} &= e^{-ik_x a + k_y a}, \quad M_{6,9} = -e^{ik_3 a} \sin \frac{\theta_3}{2}, \quad M_{6,10} = -e^{-ik_3 a} \cos \frac{\theta_3}{2}, \quad M_{6,11} = e^{ik_4 a} \cos \frac{\theta_4}{2}, \quad M_{6,12} = e^{-ik_4 a} \sin \frac{\theta_4}{2}, \\
M_{7,1} &= M_{7,2} = M_{7,3} = M_{7,4} = M_{7,5} = M_{7,6} = M_{7,7} = M_{7,8} = 0, \quad M_{7,9} = e^{ik_3 b_1} \cos \frac{\theta_3}{2}, \quad M_{7,10} = e^{-ik_3 b_1} \sin \frac{\theta_3}{2}, \\
M_{7,11} &= e^{ik_4 b_1} \sin \frac{\theta_4}{2}, \quad M_{7,12} = e^{-ik_4 b_1} \cos \frac{\theta_4}{2}, \\
M_{8,1} &= M_{8,2} = M_{8,3} = M_{8,4} = M_{8,5} = M_{8,6} = M_{8,7} = M_{8,8} = 0, \quad M_{8,9} = e^{ik_3 b_1} \sin \frac{\theta_3}{2}, \quad M_{8,10} = e^{-ik_3 b_1} \cos \frac{\theta_3}{2}, \\
M_{8,11} &= -e^{ik_4 b_1} \cos \frac{\theta_4}{2}, \quad M_{8,12} = -e^{-ik_4 b_1} \sin \frac{\theta_4}{2}, \\
M_{9,1} &= ik_1 e^{-ik_1 a} \cos \frac{\theta_1}{2}, \quad M_{9,2} = -ik_1 e^{ik_1 a} \sin \frac{\theta_1}{2}, \quad M_{9,3} = ik_2 e^{-ik_2 a} \sin \frac{\theta_2}{2}, \quad M_{9,4} = -ik_2 e^{ik_2 a} \cos \frac{\theta_2}{2}, \\
M_{9,5} &= -(ik_x - k_y) e^{-ik_x a + k_y a}, \quad M_{9,6} = (ik_x + k_y) Re^{-i\Phi + ik_x a + k_y a}, \quad M_{9,7} = -(ik_x + k_y) e^{-ik_x a - k_y a}, \\
M_{9,8} &= (ik_x - k_y) Re^{i\Phi + ik_x a - k_y a}, \quad M_{9,9} = M_{9,10} = M_{9,11} = M_{9,12} = 0, \\
M_{10,1} &= ik_1 e^{-ik_1 a} \sin \frac{\theta_1}{2}, \quad M_{10,2} = -ik_1 e^{ik_1 a} \cos \frac{\theta_1}{2}, \quad M_{10,3} = -ik_2 e^{-ik_2 a} \cos \frac{\theta_2}{2}, \quad M_{10,4} = ik_2 e^{ik_2 a} \sin \frac{\theta_2}{2}, \\
M_{10,5} &= -(ik_x - k_y) Re^{i\Phi - ik_x a + k_y a}, \quad M_{10,6} = (ik_x + k_y) e^{ik_x a + k_y a}, \quad M_{10,7} = -(ik_x + k_y) Re^{-i\Phi - ik_x a - k_y a}, \\
M_{10,8} &= (ik_x - k_y) e^{ik_x a - k_y a}, \quad M_{10,9} = M_{10,10} = M_{10,11} = M_{10,12} = 0, \\
M_{11,1} &= M_{11,2} = M_{11,3} = M_{11,4} = 0, \quad M_{11,5} = (ik_x - k_y) e^{ik_x a - k_y a}, \quad M_{11,6} = (-ik_x - k_y) Re^{-i\Phi - ik_x a - k_y a}, \\
M_{11,7} &= (ik_x + k_y) e^{ik_x a + k_y a}, \quad M_{11,8} = (-ik_x + k_y) Re^{i\Phi - ik_x a + k_y a}, \quad M_{11,9} = -ik_3 e^{ik_3 a} \cos \frac{\theta_3}{2}, \\
M_{11,10} &= ik_3 e^{-ik_3 a} \sin \frac{\theta_3}{2}, \quad M_{11,11} = -ik_4 e^{ik_4 a} \sin \frac{\theta_4}{2}, \quad M_{11,12} = ik_4 e^{-ik_4 a} \cos \frac{\theta_4}{2}, \\
M_{12,1} &= M_{12,2} = M_{12,3} = M_{12,4} = 0, \quad M_{12,5} = (ik_x - k_y) Re^{i\Phi + ik_x a - k_y a}, \quad M_{12,6} = (-ik_x - k_y) e^{-ik_x a - k_y a}, \\
M_{12,7} &= (ik_x + k_y) Re^{-i\Phi + ik_x a + k_y a}, \quad M_{12,8} = (-ik_x + k_y) e^{-ik_x a + k_y a}, \quad M_{12,9} = -ik_3 e^{ik_3 a} \sin \frac{\theta_3}{2}, \\
M_{12,10} &= ik_3 e^{-ik_3 a} \cos \frac{\theta_3}{2}, \quad M_{12,11} = ik_4 e^{ik_4 a} \cos \frac{\theta_4}{2}, \quad M_{12,12} = -ik_4 e^{-ik_4 a} \sin \frac{\theta_4}{2}. \tag{A5}
\end{aligned}$$

[1] M. A. Nielsen and I. L. Chuang, *Quantum Computations and Quantum Information* (Cambridge University Press, Cambridge, England, 2002).

[2] T. D. Ladd, F. Jelezko, R. Laflamme, Y. Nakamura, C. Monroe, and J. L. O'Brien, *Nature* **464**, 45 (2010).

[3] D. Loss and D. P. DiVincenzo, *Phys. Rev. A* **57**, 120 (1998).

[4] R. Hanson, L. P. Kouwenhoven, J. R. Petta, S. Tarucha, and L. M. K. Vandersypen, *Rev. Mod. Phys.* **79**, 1217 (2007).

[5] J. R. Petta, A. C. Johnson, J. M. Taylor, E. A. Laird, A. Yacoby, M. D. Lukin, C. M. Marcus, M. P. Hanson, and A. C. Gossard, *Science* **309**, 2180 (2005).

[6] F. H. Koppens, C. Buizert, K.-J. Tielrooij, I. T. Vink, K. C. Nowack, T. Meunier, L. Kouwenhoven, and L. Vandersypen, *Nature* **442**, 766 (2006).

[7] G. Burkard, D. Loss, and D. P. DiVincenzo, *Phys. Rev. B* **59**, 2070 (1999).

[8] M. D. Shulman, O. E. Dial, S. P. Harvey, H. Bluhm, V. Umansky, and A. Yacoby, *Science* **336**, 202 (2012).

[9] I. Buluta, S. Ashhab, and F. Nori, *Reports on Progress in Physics* **74**, 104401 (2011).

[10] O. Astafiev, Y. A. Pashkin, Y. Nakamura, T. Yamamoto, and J. S. Tsai, *Phys. Rev. Lett.* **93**, 267007 (2004).

[11] J. Q. You, X. Hu, S. Ashhab, and F. Nori, *Phys. Rev. B* **75**, 140515 (2007).

[12] A. Bermeister, D. Keith, and D. Culcer, *Applied Physics Letters* **105**, 192102 (2014).

[13] A. Kha, R. Joynt, and D. Culcer, *Applied Physics Letters* **107**, 172101 (2015).

[14] E. Paladino, Y. M. Galperin, G. Falci, and B. L. Altshuler, *Rev. Mod. Phys.* **86**, 361 (2014).

[15] S. W. Jung, T. Fujisawa, Y. Hirayama, and Y. H. Jeong, *Applied Physics Letters* **85**, 768 (2004).

[16] J. Bylander, S. Gustavsson, F. Yan, F. Yoshihara, K. Harrabi, G. Fitch, D. G. Cory, Y. Nakamura, J.-S. Tsai, and W. D. Oliver, *Nature Physics* **7**, 565 (2011).

[17] A. V. Kuhlmann, J. Houel, A. Ludwig, L. Greuter, D. Reuter, A. D. Wieck, M. Poggio, and R. J. Warburton, *Nature Physics* **9**, 570 (2013).

[18] K. W. Chan, W. Huang, C. H. Yang, J. C. C. Hwang, B. Hensen, T. Tanttu, F. E. Hudson, K. M. Itoh, A. Laucht, A. Morello, and A. S. Dzurak, *Phys. Rev. Applied* **10**, 044017 (2018).

[19] E. Kawakami, T. Jullien, P. Scarlino, D. R. Ward, D. E. Savage, M. G. Lagally, V. V. Dobrovitski, M. Friesen, S. N. Coppersmith, M. A. Eriksson, and L. M. K. Vandersypen, *Proceedings of the National Academy of Sciences* **113**, 11738 (2016).

[20] J. Yoneda, K. Takeda, T. Otsuka, T. Nakajima, M. R. Delbecq, G. Allison, T. Honda, T. Kodera, S. Oda, Y. Hoshi, *et al.*, *Nature nanotechnology* **13**, 102 (2018).

[21] R. Li, *Physica Scripta* **94**, 085808 (2019).

[22] Y. A. Bychkov and E. I. Rashba, *Journal of Physics C: Solid State Physics* **17**, 6039 (1984).

[23] V. N. Golovach, M. Borhani, and D. Loss, *Phys. Rev. B* **74**, 165319 (2006).

[24] K. C. Nowack, F. H. L. Koppens, Y. V. Nazarov, and L. M. K. Vandersypen, *Science* **318**, 1430 (2007).

[25] R. Li, J. Q. You, C. P. Sun, and F. Nori, *Phys. Rev. Lett.* **111**, 086805 (2013).

[26] D. V. Khomitsky, E. A. Lavrukhina, and E. Y. Sherman, *Phys. Rev. B* **99**, 014308 (2019).

[27] R. Li, *Journal of Physics: Condensed Matter* **30**, 395304 (2018).

[28] E. Kawakami, P. Scarlino, D. Ward, F. Braakman, D. Savage, M. Lagally, M. Friesen, S. Coppersmith, M. Eriksson, and L. Vandersypen, *Nature nanotechnology* **9**, 666 (2014).

[29] X. Hu, Y.-x. Liu, and F. Nori, *Phys. Rev. B* **86**, 035314 (2012).

[30] K. D. Petersson, L. W. McFaul, M. D. Schroer, M. Jung, J. M. Taylor, A. A. Houck, and J. R. Petta, *Nature* **490**, 380 (2012).

[31] T. Hayashi, T. Fujisawa, H. D. Cheong, Y. H. Jeong, and Y. Hirayama, *Phys. Rev. Lett.* **91**, 226804 (2003).

[32] C. L. Romano, P. I. Tamborenea, and S. E. Ulloa, *Phys. Rev. B* **74**, 155433 (2006).

[33] P. Stano and J. Fabian, *Phys. Rev. B* **72**, 155410 (2005).

[34] J. Gorman, D. G. Hasko, and D. A. Williams, *Phys. Rev. Lett.* **95**, 090502 (2005).

[35] D. V. Khomitsky, L. V. Gulyaev, and E. Y. Sherman, *Phys. Rev. B* **85**, 125312 (2012).

[36] A. Barenco, D. Deutsch, A. Ekert, and R. Jozsa, *Phys. Rev. Lett.* **74**, 4083 (1995).

[37] K. D. Petersson, J. R. Petta, H. Lu, and A. C. Gossard, *Phys. Rev. Lett.* **105**, 246804 (2010).

[38] W. M. Witzel and S. Das Sarma, *Phys. Rev. B* **74**, 035322 (2006).

[39] W. Yao, R.-B. Liu, and L. J. Sham, *Phys. Rev. B* **74**, 195301 (2006).

[40] F. H. L. Koppens, K. C. Nowack, and L. M. K. Vandersypen, *Phys. Rev. Lett.* **100**, 236802 (2008).

[41] R. Li, *Phys. Rev. B* **97**, 085430 (2018).

[42] R. Li, Z. H. Liu, Y. Wu, and C. S. Liu, *Sci Rep* **8**, 7400 (2018).

[43] Z. H. Liu and R. Li, *AIP Advances* **8**, 075115 (2018).

[44] L. D. Landau and E. M. Lifshitz, *Quantum Mechanics* (Pergamon, New York, 1965).

[45] R. Winkler, *Spin-Orbit Effects in Two-Dimensional Electron and Hole Systems* (Springer, Berlin, 2003).

[46] S. Nadj-Perge, S. M. Frolov, E. P. A. M. Bakkers, and L. P. Kouwenhoven, *Nature* **468**, 1084 (2010).

[47] S. Nadj-Perge, V. S. Pribiag, J. W. G. van den Berg, K. Zuo, S. R. Plissard, E. P. A. M. Bakkers, S. M. Frolov, and L. P. Kouwenhoven, *Phys. Rev. Lett.* **108**, 166801 (2012).

[48] E. N. Bulgakov and A. F. Sadreev, *Journal of Experimental and Theoretical Physics Letters* **73**, 505 (2001).

[49] E. Tsitsishvili, G. S. Lozano, and A. O. Gogolin, *Phys. Rev. B* **70**, 115316 (2004).

[50] J. W. G. van den Berg, S. Nadj-Perge, V. S. Pribiag, S. R. Plissard, E. P. A. M. Bakkers, S. M. Frolov, and L. P. Kouwenhoven, *Phys. Rev. Lett.* **110**, 066806 (2013).

[51] M. Trif, V. N. Golovach, and D. Loss, *Phys. Rev. B* **77**, 045434 (2008).

[52] M. P. Nowak and B. Szafran, *Phys. Rev. B* **87**, 205436 (2013).

[53] J. Romhanyi, G. Burkard, and A. Palyi, *Phys. Rev. B* **92**, 054422 (2015).

[54] P. Huang and X. Hu, *Phys. Rev. B* **89**, 195302 (2014).

[55] P. Dutta and P. M. Horn, *Rev. Mod. Phys.* **53**, 497 (1981).

- [56] M. B. Weissman, *Rev. Mod. Phys.* **60**, 537 (1988).
- [57] M. O. Scully and M. S. Zubairy, *Quantum optics* (Cambridge University Press, Cambridge, England, 1997).
- [58] G. M. Palma, K.-A. Suominen, and A. Ekert, *Proc. R. Soc. Lond. A* **452**, 567 (1996).
- [59] J. Schriefl, Y. Makhlin, A. Shnirman, and G. Schön, *New Journal of Physics* **8**, 1 (2006).
- [60] Z.-H. Liu, R. Li, X. Hu, and J. Q. You, *Scientific Reports* **8**, 2302 (2018).